8092 *Inorg. Chem.* **2009**, *48*, 8092–8105
DOI: 10.1021/ic801500x

Inorganic Chemistry
Article

pH-Dependent Syntheses, Structural and Spectroscopic Characterization, and Chemical Transformations of Aqueous Co(II)−Quinate Complexes: An Effort to Delve into the Structural Speciation of the Binary Co(II)−Quinic Acid System

M. Menelaou,[†] A. Konstantopai,[†] C. Mateescu,[⊥] H. Zhao,[‡] C. Drouza,[§] N. Lalioti,[∥] and A. Salifoglou*[,†]

[†]*Department of Chemical Engineering, Aristotle University of Thessaloniki, Thessaloniki 54124, Greece,* [‡]*Department of Chemistry, University of Puerto Rico, San Juan, Puerto Rico 00931-3346,* [§]*Department of Agricultural Production and Food Science and Technology, Cyprus University of Technology, Limassol 3603, Cyprus,* [∥]*Department of Chemistry, University of Patras, Patras 26500, Greece, and* [⊥]*Banat's University of Agricultural Sciences and Veterinary Medicine, Timisoara 300645, Romania*

Received August 7, 2008

Cobalt(II) is an essential metal ion, which can react with biologically relevant substrates in aqueous media, affording discrete soluble forms. D-(−)-quinic acid is a representative metal ion binder, capable of promoting reactions with Co(II) under pH-specific conditions, leading to the isolation of the new species $K[Co(C_7H_{11}O_6)_3]\cdot 3CH_3CH_2OH$ (**1**), $Na[Co(C_7H_{11}O_6)_3]\cdot 3CH_3CH_2OH\cdot 2.25H_2O$ (**2**), and $[Co(C_7H_{11}O_6)_2(H_2O)_2]\cdot 3H_2O$ (**3**). Compounds **1**−**3** were characterized by elemental analysis, spectroscopic techniques (Fourier-transform infrared, UV−visible, electron paramagnetic resonance (EPR), electrospray ionization mass spectrometry), magnetic studies, and X-ray crystallography. Compound **1** crystallizes in the cubic space group $P2_13$, with a = 15.3148(19) Å, V = 3592.0(8) Å^3, and Z = 4. Compound **2** crystallizes in the orthorhombic space group $P2_12_12_1$, with a = 14.9414(8) Å, b = 15.9918(9) Å, c = 16.0381(9) Å, V = 3832.1(4) Å^3, and Z = 4. Compound **3** crystallizes in the monoclinic space group $P2_1/m$, with a = 13.2198(10) Å, b = 5.8004(6) Å, c = 15.3470(12) Å, β = 108.430(7), V = 1116.45(17) Å^3, and Z = 4. The lattices in 1−**3** reveal the presence of mononuclear Co(II) units bound exclusively to quinate (**1** and **2**) or quinate and water ligands (**3**), thus projecting the unique chemical reactivity in each investigated system and suggesting that **3** is an intermediate in the synthetic pathway leading to **1** and **2**. The octahedral sites of Co(II) are occupied by oxygens, thereby reflecting the nature of interactions between the divalent metal ion and quinic acid. The magnetic and EPR data on **1** and 3 support the presence of a high-spin octahedral Co(II) in an oxygen environment, having a ground state with an effective spin of S = 1/2. The significance of **3** is further reflected into the aqueous speciation of the binary Co(II)−quinic acid system, in which **3** appears as a competent participant linked to the solid state species **1**. The physicochemical profiles of **1**−**3**, in the solid state and in solution, earmark the importance of aqueous structural speciation, which projects chemical reactivity pathways in the binary Co(II)−quinate system, involving soluble Co(II) forms emerging through interactions with low molecular mass O-containing physiological substrates, such as quinic acid.

Introduction

The importance of cobalt in human physiology has been recognized, despite its low availability in the earth's crust. Cobalt has been found to exist in biota as a metal cofactor, required for a specific group of enzymatic systems. Outstanding among such systems stand the B_{12} coenzyme and vitamin B_{12}[1−4] and cobalt-containing biomolecules such as metallohydrolases, including aminopeptidase,[5] nitrile hydratases,[6] ribonucleotide reductase, glutamate mutase, and others.[7] On the other hand, the absence of cobalt appears to be a cause for pathophysiologically aberrant conditions such as anemias.[8] In contrast to this ostensibly important biological role, excess amounts of that metal have been

*Author to whom correspondence should be addressed. Tel.: +30-2310-996-179. Fax: +30-2310-996-196. E-mail: salif@auth.gr.

(1) Taylor, D. M.; Williams, D. R. In *Trace Element Medicine and Chelation Therapy*; Royal Society of Chemistry: Cambridge, U. K., 1995.
(2) Balachandran, S.; Vishwakarma, R. A.; Monaghan, S. M.; Prelle, A.; Stamford, N. P. J.; Leeper, F. J.; Battersby, A. R. *J. Chem. Soc., Perkin Trans.* **1994**, *1*, 487–491.
(3) Battersby, A. R. *Acc. Chem. Res.* **1993**, *26*, 15–21.
(4) Debussche, L.; Couder, M.; Thibaut, D.; Cameron, B.; Crouzet, J.; Blanche, F. *J. Bacteriol.* **1992**, *22*, 7445–7451.
(5) (a) Roderick, S. L.; Matthews, B. W. *Biochemistry* **1993**, *32*, 3907–3912. (b) Ben-Bassat, A.; Bauer, K.; Chang, S.-Y.; Myambo, K.; Boosman, A.; Chang, S. *J. Bacteriol.* **1987**, *169*, 751–757.
(6) Payne, M. S.; Wu, S.; Fallon, R. D.; Tudor, G.; Stieglitz, B.; Turner, I. M.; Nelson, M. J. *Biochemistry* **1997**, *36*, 5447–5454.
(7) Lippard, S. J.; Berg, J. M. In *Principles of Bioinorganic Chemistry*; U. Science Books: M. Valley, CA, 1994; Ch. 11, pp 336−347.
(8) Hamilton, E. M. N.; Gropper, S. A. S. In *The Biochemistry of Human Nutrition*; West Publishing Company: New York, 1987; pp 298−301.

 Published on Web 08/06/2009

shown to induce toxic effects, manifested through elevated formation of red corpuscles and heart disease.[9,10] Cobalt salts have also been reported to (a) exert carcinogenic activity and (b) cause DNA strand breaks in animal cell cultures.

In all of the aforementioned biological systems, metal ions are mobilized toward interactions with organic substrates. In so doing, they form soluble bioavailable species with target ligands of both low and high molecular mass. One such representative substrate is the low molecular mass binder D-(−)-quinic acid, 1α,3α,4α,5β-tetrahydroxy-1-cyclohexane carboxylic acid. The molecular formula of D-(−)-quinic acid is shown in reaction 1. As a natural substrate, quinic acid can be found in plants and fruit.[11] To this end, various types of actinidia fruit contain quinic acid in concentrations (mM) comparable to two characteristic α-hydroxy carboxylate physiological binders: (a) citric acid and (b) malic acid.[12] Quinic acid is a precursor of shikimic acid,[13] which is involved in the biosynthesis of aromatic amino acids. In that respect, quinic acid appears to be vital to cellular physiology.[13,14] It is a polyfunctional organic ligand, containing two very important structural features that render it an efficient metal ion binder: (a) a carboxylate moiety known to promote metal ion binding and (b) alcoholic moieties, one of which is in an α position to the carboxylate group and three abutting alcoholic groups diametrically opposed to the carboxylate moiety, akin to polyol functionalities. On the basis of these properties, quinic acid can bind metal ions, such as Co(II), promoting solubilization through formation of discrete complexes. In this regard, investigation of the aqueous chemistry of Co(II) with α-hydroxycarboxylate binders, such as D-(−)-quinic acid, can shed light on the nature of the binary interactions and the physicochemical profile of binary Co(II)−quinate species emerging as a function of pH and molecular stoichiometry. To this end, delineation of the structural speciation of this aqueous binary system and the properties of the participating species emerge as significant steps toward understanding the role of that metal ion in the chemistry with substrates of physiological origin. Prompted by that need, we report herein (a) aqueous solution speciation studies on the binary Co(II)−quinate system; (b) the pH-dependent syntheses, isolation, spectroscopic, and structural characterization, as well as magnetic studies, for new species arising from the binary Co(II)−quinic acid system; (c) chemical reactivity and transformation studies among Co(II)−quinate species, projecting pH-specific synthetic convertibility of well-defined Co(II)−quinate species, including potential solution speciation participants; and (d) the implications of the physicochemical attributes of such species in understanding the nature of interactions and reactivity of that metal ion toward O-containing targets of biological origin.

Experimental Section

Materials and Methods. All manipulations were carried out under aerobic conditions. $Co(NO_3)_2 \cdot 6H_2O$ was purchased from BDH Chemicals, Ltd. $Co(CH_3COO)_2 \cdot 4H_2O$ was purchased from RP Carlo Erba, and D-(−)-quinic acid and $CoCl_2 \cdot 6H_2O$ were purchased from Fluka. Ammonia was purchased from RP Carlo Erba, and ethanol was purchased from PA Panreac. KOH and NaOH were supplied by Fluka. Nanopure-quality water was used for all reactions run.

Physical Measurements. Fourier-transform infrared (FT-IR) measurements were taken on a 1760X FT-Infra Red spectrometer from Perkin-Elmer, using KBr pellets. UV/visible measurements were carried out on a Hitachi U2001 spectrophotometer in the range from 190 to 1000 nm. A ThermoFinnigan Flash EA 1112 CHNS elemental analyzer was used for the simultaneous determination of carbon and hydrogen (%). The analyzer is based on the dynamic flash combustion of the sample (at 1800 °C) followed by reduction, trapping, complete gas chromatography separation, and detection of the products. The instrument is (a) fully automated and controlled by a PC via the Eager 300 dedicated software, and (b) capable of handling solid, liquid, or gaseous substances.

Electrospray ionization mass spectrometry (ESI-MS) infusion experiments were carried out by using a ThermoFisher Scientific (Bremen, Germany) model LTQ Orbitrap Discovery MS. All aqueous solutions (A = Co(II), B = quinic acid; compound **3** dissolved in water) were introduced into the ESI source of the MS at a flow rate of 3 μL/min by using an integrated syringe pump. The infusion experiments were run using a standard ESI source operating in a positive ionization mode. Source operating conditions were 3.7 kV spray voltage, 275 °C heated capillary temperature, and 12 ψ sheath gas pressure. Full-scan MS analysis was performed in profile mode using the Orbitrap mass analyzer at a mass resolving power of 30 000 (fwhm, at m/z 400), followed by data-dependent MS/MS on the top five most intense ions from the full scan. Data-dependent MS/MS analysis was performed in parallel with the MS analysis, in a centroid mode, using the LTQ mass analyzer. All accurate mass measurements of the [M + H] ions were carried out by scanning from 150 to 470 m/z. Automatic gain control (AGC) of the linear ion trap was switched on. The AGC target value was 10 000 accumulated ions for the linear ion trap and 500 000 accumulated ions for the Orbitrap. The Orbitrap was calibrated 2 h prior to the infusion experiments by using a mixture of caffeine, MRFA peptide, and Ultramark 1600. Data were acquired in an external calibration mode. The Mass Frontier (HighChem, Slovakia) software was used to confirm a suggested compound identity and structure based on observed fragmentation patterns.

The electron paramagnetic resonance (EPR) spectra of complexes **1** and **3** in the solid state and in frozen aqueous solutions were recorded on a Bruker ER 200D-SRC X-band spectrometer, equipped with an Oxford ESR 9 cryostat at 9.174 GHz, 10 dB (2mW), and temperatures below 70 K. Magnetic susceptibility data were collected on powdered samples of **1** and **3** with a Quantum Design SQUID susceptometer in the temperature ranges 2−300 K (**1**) and 1.7−300 K (**3**), respectively, under various applied magnetic fields. Magnetization measurements were carried out at three different temperatures in the field range 0−5 T.

pH-Potentiometric Measurements. The protonation constants of quinic acid were determined by pH-potentiometric titrations of 30 mL samples in the pH range 2.8−13 under a purified argon atmosphere. The concentration of quinic acid was in the range of 1.7−7.0 mmol dm^{-3}. The stability constants

(9) Helis, H. M.; de Meester, P.; Hodgson, D. J. *J. Am. Chem. Soc.* **1976**, *99*, 3309–3312.
(10) Waldbott, G. L. In *Health Effects of Environmental Pollutants*; Mosby, C. V. Co.: St. Louis, MO, 1973.
(11) Hulme, A. C.; Wooltorton, L. S. C. *J. Sci. Food Agric.* **1957**, *8*, 117–122.
(12) Okamoto, G.; Goto, S. *Scientific Reports of the Faculty of Agriculture*; Okayama University: Okayama, Japan, 2005; Vol. *94*, pp 9−13.
(13) (a) Haslam, E. *Shikimic Acid: Metabolism and Metabolites*; Wiley & Sons: New York, 1993.(b) Pittard, A. J. In *Escherichia coli and Salmonella: Cellular and Molecular Biology*; Neidhardt, F. C., Ed.; ASM Press: Washington, DC, 1996; Chapter 28.
(14) Bentley, R. *Crit. Rev. Biochem. Mol. Biol.* **1990**, *25*, 307–384.

of the complexes between Co(II) and quinic acid were determined by pH-potentiometric titrations of 30 mL samples in the pH range 2.5−8.4 under a purified argon atmosphere. Precipitation was observed at a pH of about 8.4, in line with previously reported behavior of the aqueous system of Co(II) with some aminodiphosphonic acids.[15]

All solutions were prepared using Fluka reagent-grade quinic acid, $CoCl_2 \cdot 6H_2O$, and ultrapure deionized water. The purity of quinic acid and the exact concentration of quinate and Co(II) solutions, were determined by the Gran method.[16] To pursue the speciation study at pH values less than 2.8, known amounts of nitric acid (0.01 M) were added in the systems under investigation. The exact concentration of Co(II) was checked by the method of Kinnunen and Wennerstrand.[17]

The ionic strength was adjusted to 0.15 M with NaCl. The temperature was maintained at 25.0 ± 0.1 °C during the measurements. The titrations were carried out with a carbonate-free NaOH solution of known concentration (ca. 0.15 M). The NaOH solution was standardized using potassium hydrogen iodate ($KH(IO_3)_2$). The ligand concentration was 1.7 mM, and the employed metal/ligand ratios were 1:1, 1:2, 1:3, and 1:4. The pH was monitored with a computer-controlled Crison titration system elaborated for titrations at low concentrations[18] and a Mettler Toledo-Inlab 412 combined glass-electrode, calibrated for hydrogen ion concentration according to Irving et al.,[19] by using the GLEE program.[20] The ionic product of water was found to be $pK_w = 13.76$.

The stepwise protonation constants of quinic acid are given as $\log K_n$ ($n = 1, 2$), consistent with the equilibrium $H_{n-1}L + H \rightleftarrows H_nL$, where $K_n = [H_nL]/[H_{n-1}L][H]$. The initial computations were obtained in the form of overall protonation constants $\beta_n = [H_nL]/[L][H]^n$, taking into account that $\beta_n = \Pi_{n=1}^{n=2} K_n$. The concentration stability constants $\beta_{pqr} = [M_pL_qH_r]/[M]^p[L]^q[H]^r$ for quinic acid were calculated with Superquad[21] and, for Co(II)−quinate complexes, emerging in the investigated system, with the PSEQUAD computer program.[22] Species distribution diagrams were computed from the overall formation constants with HySS.[23]

Formation of hydroxo complexes of Co(II) was taken into consideration in the employed calculations. The stability constants used for the hydroxo species of Co(II) were taken from the data of Baes and Mesmer[24] and corrected for an ionic strength of 0.15 M, using the Davies equation: $[CoH_{-1}]^+$ ($\log \beta_{1-1} = -9.40$), $[Co_2H_{-1}]^{3+}$ ($\log \beta_{2-2} = -10.91$), $[CoH_{-2}]^0$ ($\log \beta_{1-2} = -18.54$).[25]

Synthesis of $K[Co(C_7H_{11}O_6)_3] \cdot 3CH_3CH_2OH$ (1). $Co(NO_3)_2 \cdot 6H_2O$ (0.50 g, 1.7 mmol) and D-(−)-quinic acid (0.97 g, 5.0 mmol) were placed in a 25 mL round-bottom flask and dissolved in 6 mL of water. The reaction mixture was then stirred at room temperature until both reactants were completely dissolved. Subsequently, the pH of the clear solution was adjusted to 5 with KOH. The resulting reaction mixture was placed in the refrigerator at 4 °C. The addition of ethanol afforded, a few months later, pink crystalline material, which appeared on the bottom of the flask. The crystalline product was isolated by filtration and dried in vacuo. Yield: 0.57 g (41%). Anal. Calcd for **1**, $K[Co(C_7H_{11}O_6)_3] \cdot 3CH_3CH_2OH$ ($C_{27}H_{51}O_{21}KCo$, MW = 809.71): C, 40.00; H, 6.30. Found: C, 39.65; H, 6.24.

Synthesis of $Na[Co(C_7H_{11}O_6)_3] \cdot 3CH_3CH_2OH \cdot 2.25H_2O$ (2). $CoCl_2 \cdot 6H_2O$ (0.50 g, 2.1 mmol) and D-(−)-quinic acid (0.97 g, 5.0 mmol) were placed in a 25 mL round-bottom flask and dissolved in 6 mL of water. The reaction mixture was then stirred at room temperature until both reactants were completely dissolved. Subsequently, the pH of the clear solution was adjusted to 5 with NaOH. The resulting reaction mixture was placed in the refrigerator at 4 °C. The addition of ethanol afforded, a few months later, a pink crystalline material, which appeared on the bottom of the flask. The crystalline product was isolated by filtration and dried in vacuo. Yield 0.43 g (26%). Anal. Calcd for **2**, $Na[Co(C_7H_{11}O_6)_3] \cdot 3CH_3CH_2OH \cdot 2.25H_2O$ ($C_{27}H_{55.50}CoNaO_{23.25}$, MW = 834.2): C, 38.87; H, 6.70. Found: C, 38.66; H, 6.53.

Synthesis of $[Co(C_7H_{11}O_6)_2(H_2O)_2] \cdot 3H_2O$ (3). A quantity of $Co(NO_3)_2 \cdot 6H_2O$ (0.30 g, 1.0 mmol) was dissolved in 3 mL of nanopure water in a round-bottom flask. To that solution 0.40 g (2.1 mmol) of quinic acid was added under continuous stirring. The pH of the resulting solution was raised to ∼7 with aqueous ammonia. After a short period of stirring at room temperature, the reaction mixture was placed in the refrigerator at a temperature of 4 °C. The addition of ethanol led to the precipitation of purple crystalline material, which was isolated by filtration and dried in vacuo. Yield: 0.34 g (62%). Anal. Calcd for **3** $[Co(C_7H_{11}O_6)_2(H_2O)_2] \cdot 3H_2O$ ($C_{14}H_{32}CoO_{17}$, MW = 531.32): C, 31.16; H, 6.02. Found: C, 31.41; H, 5.91%. ESI-MS (m/z = 442, $z = 1$, $[(M - 2H_2O) + H]^+$).

Transformation of $[Co(C_7H_{11}O_6)_2(H_2O)_2] \cdot 3H_2O$ (3) to $K[Co(C_7H_{11}O_6)_3] \cdot 3CH_3CH_2OH$ (1). $[Co(C_7H_{11}O_6)_2(H_2O)_2] \cdot 3H_2O$ (0.10 g, 0.19 mmol) was dissolved in 2 mL of water in a 25 mL round-bottom flask. D-(−)-quinic acid (0.040 g, 0.19 mmol) was added to it slowly and under continuous stirring. The reaction mixture was then stirred at room temperature until both reactants were completely dissolved. Subsequently, the pH of the clear solution was adjusted to 6 with aqueous KOH. The resulting reaction mixture was placed in the refrigerator at 4 °C. The addition of ethanol afforded, a few days later, pink crystalline material, which appeared on the bottom of the flask. The crystalline product was isolated by filtration and dried in vacuo. Positive identification of the product was achieved by FT-IR spectroscopy and X-ray crystallographic unit cell determination for one of the single crystals isolated. Yield: 0.060 g (40%).

Transformation of $[Co(C_7H_{11}O_6)_2(H_2O)_2] \cdot 3H_2O$ (3) to $Na[Co(C_7H_{11}O_6)_3] \cdot 3CH_3CH_2OH \cdot 2.25H_2O$ (2). $[Co(C_7H_{11}O_6)_2(H_2O)_2] \cdot 3H_2O$ (0.10 g, 0.19 mmol) was placed in a 25 mL round-bottom flask and dissolved in 2 mL of water. D-(−)-quinic acid (0.040 g, 0.19 mmol) was then added slowly and under continuous stirring. The reaction mixture was then stirred at room temperature until both reactants were completely dissolved. Then, the pH of the clear solution was adjusted to 6 with aqueous NaOH. The resulting reaction mixture was subsequently placed in the refrigerator at 4 °C. A few days later, the addition of ethanol afforded pink crystalline material, which appeared on the bottom of the flask. The crystalline product was isolated by filtration and dried in vacuo. Positive identification of the product was achieved by FT-IR spectroscopy and X-ray crystallographic unit cell determination for one of the single crystals isolated. Yield: 0.080 g (50%).

X-Ray Crystal Structure Determination. X-ray-quality crystals of compound **1** were grown from reaction mixtures upon ethanol precipitation. A single crystal with dimensions

(15) Kurzak, B.; Kamecka, A.; Kurzak, K.; Jezierska, J.; Kafarski, P. *Polyhedron* **2000**, *19*, 2083–2093.
(16) (a) Gran, G. *Acta Chem. Scand.* **1950**, *29*, 559. (b) Gran, G. *Analyst* **1952**, *77*, 661–671. (c) Rossotti, F. J. C.; Rossotti, H. *J. Chem. Educ.* **1965**, *42*, 375–378.
(17) Kinnunen, J.; Wennerstrand, B. *Chemist−Analyst* **1955**, *44*, 33.
(18) Pettit, L. D., *Molspin pH-meter Instruction Manual*; Molspin Ltd.: England.
(19) Irving, H. M.; Miles, M. G.; Petit, L. D. *Anal. Chim. Acta* **1967**, *38*, 475–479.
(20) Gans, P.; O'Sullivan, B. *Talanta* **2000**, *51*, 33–37.
(21) Gans, P.; Sabatini, A.; Vacca, A. *J. Chem. Soc., Dalton Trans.* **1985**, 1195–1200.
(22) Zékány, L.; Nagypál, I.; Peintler, G. *PSEQUAD for Chemical Equilibria*; Technical Software Distributions: Baltimore, MD, 1991.
(23) Alderighi, L.; Gans, P.; Ienco, A.; Peters, D.; Sabatini, A.; Vacca, A. *Coord. Chem. Rev.* **1999**, *184*, 311–318.
(24) (a) Lacour, S.; Deluchat, V.; Bollinger, J.-C.; Serpaud, B. *Talanta* **1998**, *46*, 999–1009. (b) Baes, C. F., Jr.; Mesmer, R. E. *The Hydrolysis of Cations*; John Wiley and Sons: New York, 1976.
(25) Colston, B. J.; Robinson, V. J. *Analyst* **1997**, *122*, 1451–1455.

$0.15 \times 0.16 \times 0.10$ mm (**1**) was mounted on the tip of a glass fiber with epoxy glue. X-ray diffraction data were collected on a Bruker AXS SMART 1K CCD area detector with graphite monochromated Mo Kα radiation (λ = 0.71073 Å), at room temperature, using the program SMART-NT.[26] The collected data were processed with SAINT-NT.[27] An empirical absorption correction was applied through the program SADABS.[27] The structure was solved by direct methods and refined by full-matrix least-squares cycles on F^2.[28] All non-hydrogen atoms were refined anisotropically. Hydrogens were geometrically positioned on carbon atoms and left riding on their parent atoms during structure refinement. Hydroxyl hydrogen-atom positions were first determined from E-maps, brought to reasonable distances from their oxygen atoms, and then fixed. The final assignment satisfies the electroneutrality of the entire compound **1**, with the understanding that cobalt ions are formally in the +2 oxidation state. Crystallographic details for **1** are summarized in Table 1. Further details on the crystallographic studies as well as atomic displacement parameters are given as Supporting Information in CIF format. Further crystallographic details for **1** are as follows: $2\theta_{max} = 56.50°$; scan speed 3.0°/min; reflections collected/unique/used = 23 499/2822/2393 [R(int) = 0.0477]; 162 parameters refined; $[\Delta\rho]_{max}/[\Delta\rho]_{min}$ = +0.255/−0.237 e/Å^3; R/R_w (for all data), 0.0489/0.0802.

X-ray-quality crystals of compounds **2** and **3** were grown from reaction mixtures upon ethanol precipitation. A single crystal with dimensions $0.17 \times 0.11 \times 0.07$ mm (**2**) and $0.28 \times 0.19 \times 0.08$ mm (**3**) was mounted on an Xcalibur Oxford diffractometer equipped with a Sapphire 3 CCD detector and a 4-cycle Kappa geometry goniometer, using an enhanced Mo X-ray source and a graphite radiation monochromator. Unit cell dimensions for **2** and **3** were determined and refined by using the angular settings of all of the reflection frames in the ranges $6.3 < 2\theta < 60.5°$ and $6.5 < 2\theta < 61.9°$, respectively. Relevant crystallographic data appear in Table 1. Intensity data were measured by using a $\theta-2\theta$ scan. Three standard frames were monitored every 35 reflections, over the course of data collection, to ensure the stability of the sample. An analytical absorption correction was applied using CrysAlis RED software. Further crystallographic details for **2** are as follows: $2\theta_{max}$ = 60.5°; reflections collected/unique/used, = 32 253/10 379/7358 [R(int) = 0.0493]; 507 parameters refined; $[\Delta/\sigma]_{max}$ = 0.066; $[\Delta\rho]_{max}/[\Delta\rho]_{min}$ = +0.881/−0.461 e/Å^3; R/R_w (for all data), 0.0533/0.0841; and R/R_w (final indices [$I > 2\sigma(I)$]), 0.0381/0.0824. Further crystallographic details for **3** are as follows: $2\theta_{max}$ = 61.9°; reflections collected/unique/used = 16 270/5938/5607 [R(int) = 0.0173]; 321 parameters refined; $[\Delta/\sigma]_{max}$ = 0.078; $[\Delta\rho]_{max}/[\Delta\rho]_{min}$ = +1.596/−0.663 e/Å^3; R/R_w (for all data), 0.0554/0.1410. CrysAlis CCD and CrysAlis RED software were used for computing data collection and computing data reduction/cell refinement, respectively.[29] The structure was solved with direct methods and refined by full-matrix least-squares techniques on F^2 by using SHELXS-97.[30] Special computing molecular graphics incorporated in the WinGX 3.2 interface were used.[31] All of the non-H atoms were refined anisotropically. The methylene hydrogen atoms of the quinate ligand were introduced at calculated positions as riding on bonded atoms. The remainder of the hydrogen atoms were located by difference Fourier maps and were refined isotropically.

(26) *SMART-NT*, version 5.0; Bruker AXS: Madison, WI, 1998.
(27) *SAINT-NT*, version 5/6.0; Bruker AXS: Madison, WI, 1999.
(28) *SHELXTL-NT*, version 5.1; Bruker AXS: Madison, WI, 1998.
(29) (a) *CrysAlis CCD*, version 1.171.29.9, release 23−03−2006; Oxford Diffraction Ltd.: Oxfordshire, U.K., **2006**. (b) *CrysAlis.NET*; *CrysAlis RED*, version 1.171.29.9, release 23-03-2006; Oxford Diffraction Ltd.: Oxfordshire, U.K., **2006**.
(30) (a) Sheldrick, G. M. *SHELX-97*; University of Göttingen: Göttingen, Germany, 1997. (b) Sheldrick, G. M. *SHELX-97*, release 97-2; University of Göttingen: Göttingen, Germany, 1993−7.
(31) Farrugia, L. J. *J. Appl. Crystallogr.* **1999**, *32*, 837–838.

Results

Synthesis. Compounds **1** and **2** were synthesized in an aqueous solution through simple reactions between Co(II) and quinic acid, employing a 1:3 molar ratio. In both cases, the adjustment of pH was achieved by adding KOH and NaOH, respectively, to reach a final value of 5.0. The employment of KOH and NaOH, as bases, was crucial in each investigated reaction. Not only did they help adjust the pH of the reaction mixture but they also provided the appropriate counterions needed to balance the negative charge on the arisen anionic complex. Furthermore, the addition of ethanol was also crucial in achieving the lattice of **1** and **2**. The stoichiometric reaction leading to the formation and isolation of compounds **1** and **2** is shown below (reaction 1):

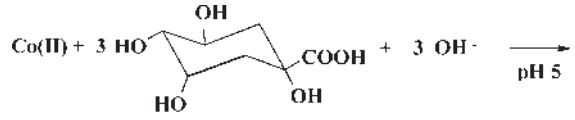

D-(-)-quinic Reaction 1

$$[Co(C_7H_{11}O_6)_3]^{-1} + 3\ H_2O$$

The resulting pink-colored crystalline Co(II)−quinate compounds were further used for spectroscopic and structural characterization purposes. Elemental analysis of the isolated crystalline products suggested the molecular formulations $K[Co(C_7H_{11}O_6)_3]\cdot 3CH_3CH_2OH$ (**1**) and $Na[Co(C_7H_{11}O_6)_3]\cdot 3CH_3CH_2OH\cdot 2.25H_2O$ (**2**). Further spectroscopic evaluation of the crystalline products by FT-IR confirmed the presence of quinate bound to Co(II) in both complexes. Finally, X-ray crystallography confirmed the analytical and spectroscopic results by providing the three dimensional structure of the crystalline products **1** and **2**.

In consonance to the aforementioned compounds **1** and **2**, compound **3** was synthesized in a pH-specific fashion by reacting Co(II) and quinic acid in a molar ratio of 1:2 in the presence of aqueous ammonia. In contrast to the previous two syntheses, in this case, ammonia served as a base, solely raising the pH of the reaction mixture to ∼7 (but not participating in the emerging lattice of the isolated crystalline product **3**). Here as well, ethanol was the precipitating agent inducing crystallization of the isolated product. The stoichiometric reaction leading to the formation and isolation of compound **3** is shown below (reaction 2):

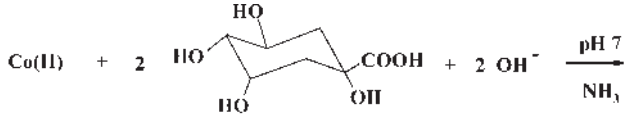

$[Co(C_7H_{11}O_6)_2(H_2O)_2]$ Reaction 2

Elemental analysis of the isolated crystalline product suggested the molecular formulation $[Co(C_7H_{11}O_6)_3(H_2O)_2]\cdot 3H_2O$ (**3**), discounting the presence of counterions from the lattice. Further confirmation of the structural identity of the species came from FT-IR spectroscopy and X-ray crystallography.

Table 1. Summary of Crystal, Intensity Collection, and Refinement Data for $K[Co(C_7H_{11}O_6)_3]\cdot 3CH_3CH_2OH$ (**1**), $Na[Co(C_7H_{11}O_6)_3]\cdot 3CH_3CH_2OH\cdot 2.25H_2O$ (**2**), and $[Co(C_7H_{11}O_6)_2(H_2O)_2]\cdot 3H_2O$ (**3**)

	1	**2**	**3**
formula	$C_{27}H_{51}CoKO_{21}$	$C_{27}H_{55.50}CoNaO_{23.29}$	$C_{14}H_{32}CoO_{17}$
fw	809.71	834.81	531.32
temp, K	298(2)	100(2)	100(2)
wavelength	Mo Kα 0.71073	Mo Kα 0.71073	Mo Kα 0.71073
space group	$P2_13$	$P2_12_12_1$	$P2_1/m$
a (Å)	15.3148(19)	14.9414(8)	13.2198(10)
b (Å)	15.3148(19)	15.9918(9)	5.8004(6)
c (Å)	15.3148(19)	16.0381(9)	15.3470(12)
β (deg)			108.430(7)
V, (Å^3)	3592.0(8)	3832.1(4)	1116.45(17)
Z	4	4	4
D_{calcd}/D_{measd} (Mg m^{-3})	1.407/1.41	1.447/1.45	1.581/1.58
abs. coeff. (μ), mm^{-1}	0.111	0.546	0.850
range of h, k, l	$-19 \le h \le +18$ $-15 \le k \le +19$ $-19 \le l \le +20$	$-20 \le h \le +16$ $-18 \le k \le +21$ $-22 \le l \le +18$	$-18 \le h \le +18$ $-8 \le k \le +8$ $-21 \le l \le +21$
goodness-of-fit on F^2	1.012	0.949	1.063
R^a	$R = 0.0378^b$	$R = 0.0381^b$	$R = 0.0351^b$
$R_w{}^a$	$R_w = 0.0802^b$	$R_w = 0.0824^b$	$R_w = 0.0967^b$

[a] R values are based on F values, R_w values are based on F^2. $R = \frac{\sum ||F_o| - |F_c||}{\sum (|F_o|)}$, $R_w = \sqrt{\frac{\sum [w(F_o^2 - F_c^2)^2]}{\sum [w(F_o^2)^2]}}$. [b] For 2393 (**1**), 7358 (**2**), and 5607 (**3**) reflections with $I > 2\sigma(I)$.

Compounds **1**−**3** are soluble in water. They are also insoluble in organic solvents, like methanol, acetonitrile, chlorinated solvents ($CHCl_3$, CH_2Cl_2), toluene, and DMF. Compounds **1**−**3** are stable in the crystalline form in the air at room temperature for long periods of time.

Transformation Chemistry. Poised to understand the association between the two different species **1** and **3**, the potential synthetic link between **1** and **3** was perused. To that end, compound **3** was dissolved in water, and 1 equiv of quinic acid was added with concurrent adjustment of the pH of the reaction mixture to the optimal value of ∼6 by the addition of MOH ($M = K^+$, Na^+; reaction 3).

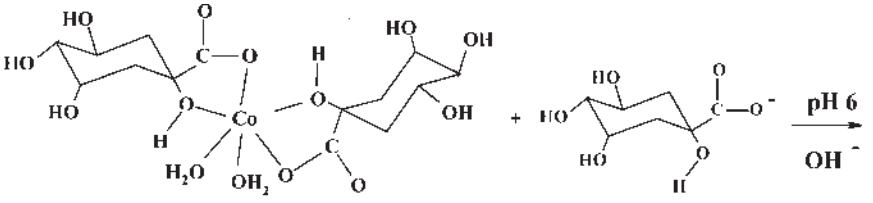

$$[Co(C_7H_{11}O_6)_3]^- + 2\ H_2O$$

Reaction 3

The addition of the precipitating agent ethanol led to the isolation of pink crystalline material. The isolated product was identified positively as compounds **1** and **2** by FT-IR spectroscopy and X-ray crystal structure determination of the cell parameters of a single crystal from the pure and homogeneous crystalline material. Through this approach, not only was compound **3** linked to compounds **1** and **2** but there was also an alternative route proven to exist for the stepwise synthesis and isolation of the $[Co(C_7H_{11}O_6)_3]^-$ anionic complex (in **1** and **2**).

Description of X-Ray Crystallographic Structures. Compounds **1** and **2** emerge from crystal lattices of discrete metal ionic complexes and counteracting ions. The ORTEP diagram of $[Co(C_7H_{11}O_6)_3]^-$ (**1**) is shown in Figure 1. A list of selected bond distances and angles for **1** and **2** is given in Table 2. Complex **1** crystallizes in the cubic space group $P2_13$ with four molecules per unit cell. Complex **2** crystallizes in the orthorhombic space group $P2_12_12_1$ with four molecules per unit cell. In both complexes **1** and **2**, the anionic metal ionic assembly is similar. Therefore, the two structures will be discussed together. Specifically, the Co(II) assembly consists of the central metal ion with three quinate ligands coordinated to it. Metal ion binding proceeds through the carboxylate and alcoholic oxygens O(5) and O(1), respectively. These two moieties bind Co(II) through formation of a five-membered cyclic ring, rendering the emerging species quite stable. Collectively, the assembly of the aforementioned quinate ligands renders the Co(II) ion six-coordinate and the geometry around it distorted octahedral.

The Co−O bond distances are in the range from 2.049(2) to 2.091(2) Å for **1** and 2.041(2) to 2.125(2) Å for **2**. These are comparable with corresponding distances in complexes $(NH_4)_4[Co(C_6H_5O_7)_2]$ (2.051(2)−2.157(2) Å) (**4**),[32] $K_2[Co_2(C_6H_5O_7)_2(H_2O)_4]\cdot 6H_2O$ (2.042(2)−2.194(2) Å) (**5**),

(32) Matzapetakis, M.; Dakanali, M.; Raptopoulou, C. P.; Tangoulis, V.; Terzis, A.; Moon, N.; Giapintzakis, J.; Salifoglou, A. *J. Biol. Inorg. Chem.* **2000**, *5*, 469–474.

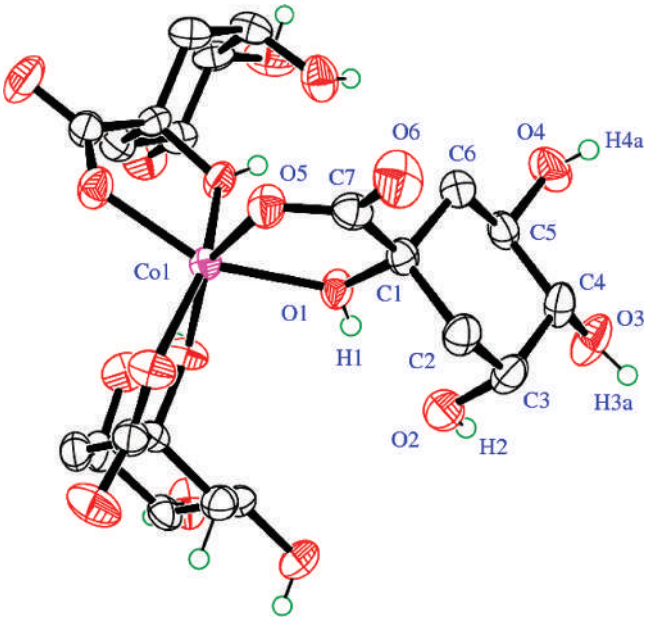

Figure 1. ORTEP diagram of the $[Co(C_7H_{11}O_6)_3]^-$ anion in **1** with the atom-labeling scheme (30% thermal probability ellipsoids).

$Na_2[Co_2(C_6H_5O_7)_2(H_2O)_4]\cdot 6H_2O$ (2.044(2)−2.169(2) Å) (**6**),[33] $[Co(C_4H_5O_5)_2(H_2O)_2]\cdot 2H_2O$ (2.066(1)−2.112(1) Å) (**7**),[34] and $[Co(CO_2CH_2CH(OH)CO_2)]\cdot 3H_2O$ (2.067(3)−2.136(3) Å) (**8**).[35]

The angles are in the range 76.36(7)−107.77(7)° for complex **1** and 76.70(6)−108.21(7)° for complex **2**, with the mean being fairly close to the ideal octahedral angle of 90°. The angle values in each case are similar to those observed in **4** (74.80(7)−105.20(7)°), **5** (77.17(7)−98.18(8)°), **6** (78.25(7)−93.43(7)°), **7** (77.03(5)−92.91(6)°), and **8** (76.82(12)−101.02(13)°) and similar to those in the quinate organic−inorganic hybrid $[Mn_2(C_7H_{11}O_6)_4]_n\cdot nH_2O$ (69.56(15)−96.75(17)° and 73.02(13)−95.41(15)°, respectively.[36]

The octahedral cobalt ion in **1** is structurally similar to other octahedral divalent metal ions such as Zn(II),[37] Cu(II),[38] and Ni(II)[39] in analogous species bearing citrates. The M−O distances observed in those complexes are in line with those seen in **1** and range from 2.052(2) to 2.164(2) Å (Zn(II)) and from 2.021(3) to 2.072(3) Å (Ni(II)), while a wider range due to Jahn−Teller distortion is observed in the copper analog (1.969(3)−2.341(3) Å). Equally comparable are the M−O distances with those occurring in the congener quinate complexes $[Zn(C_7H_{11}O_6)_2]$,[40] $[Mn_2(C_7H_{11}O_6)_4]_n\cdot nH_2O$,[36] $[Cd(C_7H_{11}O_6)_2]\cdot H_2O$, $[Cu(C_7H_{10}O_6)(H_2O)]_2\cdot 2H_2O$,[41] $\{[Cu(NO_3)(C_7H_{11}O_6)(H_2O)]\cdot 2H_2O\}_n$, $\{[CuCl(C_7H_{11}O_6)(H_2O)]\cdot H_2O\}_n$,[42] $[Pt(C_6H_{14}N_2)(C_7H_{10}O_6)]$,[43] and the trinuclear $(NH_4)_2\{[V(O)_2]_2[V(O)](\mu\text{-}C_7H_{10}O_6)_2\}\cdot H_2O$.[44]

Overall, the quinate ligand plays the role of an efficient metal ion chelator, employing a specific type of anchor available in its structure and effectively formulating the coordination environment around Co(II).

The potassium and sodium cations counterbalance efficiently the anionic charge of $[Co(C_7H_{11}O_6)_3]^-$ in complexes **1** and **2**, respectively. Each potassium ion, in the lattice in **1**, is in contact with three carboxylate oxygen atoms from three quinate molecules as well as three ethanol oxygen atoms. The K−O (carboxylate) distance is 2.650(2) Å, while that of K−O (ethanol) is 2.908(3) Å. In complex **1**, each quinate ligand bridges one Co(II) ion and one K^+ ion with a K−Co distance of 6.740(1) Å. Each Co(II) ion is connected to three K^+ ions and is located above the center of the plane defined by those three K^+ ions. Similarly, each K^+ ion is located above the center of the triangle formed by three Co(II) ions, resulting in the formation of an infinite 3D network.

The crystal structure of **2** is composed of an infinite 3D network through a three-blade left-handed propeller centered at the Na^+ ion. By analogy to complex **1**, the sodium ion in the emerging crystalline lattice is coordinated to the three quinate ligands in a Δ conformation (Figure 2A,B). Each blade consists of one Δ-Co(II) and one peripheral Δ-Na^+ ion bridged by one quinate ligand. This dimer is connected to the central Na^+ ion through a second ligand (Figure 2A). The central Na^+ ion and the three neighboring Co(II) ions define a plane, with the Na^+ ion placed 0.100(1) Å above the plane. The three peripheral Na^+ ions define a second plane parallel to the first one and located 1.532(1) Å below it (Figure 2B). Each peripheral Na^+ ion defines the center of a new propeller, which is directed perpendicularly to the original one, thus giving rise to the assembly of the 3D network. The ethanol and the water solvent molecules are distributed in the intervening space defined by the chains of the network.

In the case of compound **3**, the ORTEP diagram for $[Co(C_7H_{11}O_6)_2(H_2O)_2]$ (**3**) is shown in Figure 3. A list of selected bond distances and angles for **3** are given in Table 2. Complex **3** crystallizes in the monoclinic space group $P2_1/m$ with four molecules per unit cell. The crystal structure reveals a mononuclear assembly with a Co(II) ion at the center. Two quinate ligands bind Co(II) in a bidentate fashion, utilizing the carboxylate and alcoholic groups. As in the cases of **1** and **2**, here as well, the alcoholic oxygens retain their proton, thus rendering the quinate ligand singly deprotonated. The incipient formation of a five-membered cyclic ring for each one of the two quinates contributes to the stability of the arising complex. Two water molecules are also attached to Co(II), thus fulfilling the coordination requirements of the metal ion. In contrast to the lattices of **1** and **2**, where

(33) Kotsakis, N.; Raptopoulou, C. P.; Tangoulis, V.; Terzis, A.; Giapintzakis, J.; Jakusch, T.; Kiss, T.; Salifoglou, A. *Inorg. Chem.* **2003**, *42*, 22–31.
(34) Karipides, A. *Acta Crystallogr.* **1981**, *B37*, 1115–1117.
(35) Kryger, L.; Rasmussen, S. E. *Acta Chem. Scand.* **1972**, *26*, 2349–2359.
(36) Menelaou, M.; Raptopoulou, C. P.; Terzis, A.; Tangoulis, V.; Salifoglou, A. *Eur. J. Inorg. Chem.* **2005**, 1957–1967.
(37) Swanson, R.; Ilsley, W. H.; Stanislowski, A. G. *J. Inorg. Biochem.* **1983**, *18*, 187–194.
(38) Bott, R. C.; Sagatys, D. S.; Lynch, D. E.; Smith, G.; Kennard, C. H. L.; Mak, T. C. W. *Aust. J. Chem.* **1991**, *44*, 1495–1498.
(39) Zhou, Z.-H.; Lin, Y.-J.; Zhang, H.-B.; Lin, G.-D.; Tsai, K.-R. *J. Coord. Chem.* **1997**, *42*, 131-141.
(40) Inomata, Y.; Haneda, T.; Howell, F. S. *J. Inorg. Biochem.* **1999**, *76*, 13–17.
(41) Barba-Behrens, N.; Salazar-Garcia, F.; Bello-Ramirez, A. M.; Garcia-Baez, E.; Rosales-Hoz, M. J.; Contreras, R.; Flores-Parra, A. *Trans. Met. Chem.* **1994**, *19*, 575.
(42) Bkouche-Walksman, I. *Acta Crystallogr., Sect. C* **1994**, *50*, 62.
(43) Hata, G.; Kitano, Y.; Kaneko, T.; Kawai, H.; Mutoh, M. *Chem. Pharm. Bull.* **1992**, *40*, 1604–1605.
(44) Codd, R.; Hambley, T. W.; Lay, P. A. *Inorg. Chem.* **1995**, *34*, 877–882.

Table 2. Bond Lengths [Å] and Angles [deg] in **1**, **2**, and **3**

distances					
1		**2**		**3**	
Co(1)−O(1)	2.091(2)	Co(1)−O(1)	2.065(2)	Co(1)−O(1)	2.082(2)
Co(1)−O(5)	2.049(2)	Co(1)−O(5)	2.090(2)	Co(1)−O(2)	2.085(2)
		Co(1)−O(11)	2.125(2)	Co(1)−O(3)	2.069(3)
		Co(1)−O(15)	2.042(2)	Co(1)−O(4)	2.073(2)
		Co(1)−O(21)	2.041(2)	Co(1)−O(5)	2.041(3)
		Co(1)−O(25)	2.066(2)	Co(1)−O(6)	2.079(3)
angles					
1		**2**		**3**	
O(5)−Co(1)−O(1)	76.36(7)	O(1)−Co(1)−O(5)	76.70(6)	O(1)−Co(1)−O(2)	76.59(6)
O(5)′−Co(1)−O(5)	95.19(6)	O(15)−Co(1)−O(5)	91.22(6)	O(1)−Co(1)−O(3)	94.51(7)
O(5)−Co(1)−O(1)′	107.77 (7)	O(5)−Co(1)−O(11)	153.38(6)	O(1)−Co(1)−O(5)	96.03(7)
O(1)′−Co(1)−O(1)	84.84(7)	O(11)−Co(1)−O(1)	84.27(7)	O(1)−Co(1)−O(6)	92.29(8)
O(5)′−Co(1)−O(1)	156.03(7)	O(15)−Co(1)−O(1)	102.72(7)	O(1)−Co(1)−O(4)	158.28 (7)
		O(15)−Co(1)−O(25)	97.46(7)	O(2)−Co(1)−O(3)	94.26 (7)
		O(15)−Co(1)−O(11)	74.86(6)	O(2)−Co(1)−O(4)	84.54(6)
		O(25)−Co(1)−O(21)	77.55(7)	O(2)−Co(1)−O(5)	92.0 1(8)
		O(25)−Co(1)−O(5)	95.94(6)	O(2)−Co(1)−O(6)	168.76 (8)
		O(21)−Co(1)−O(11)	88.42(7)	O(3)−Co(1)−O(4)	76.07 (7)
		O(25)−Co(1)−O(1)	158.58(7)	O(3)−Co(1)−O(5)	168.75 (7)
		O(21)−Co(1)−O(5)	108.21 (7)	O(3)−Co(1)−O(6)	84.88 (7)
		O(21)−Co(1)−O(1)	85.61(7)	O(4)−Co(1)−O(5)	95.27(7)
		O(21)−Co(1)−O(15)	160.26(7)	O(4)−Co(1)−O(6)	106.06(8)
		O(25)−Co(1)−O(11)	108.12(7)	O(5)−Co(1)−O(6)	90.77(8)

K^+ and Na^+ ions were present, no ammonium cations were located in the arising lattice of the stable crystalline species $[Co(C_7H_{11}O_6)_2(H_2O)_2]$ (**3**).

As in the case of compounds **1** and **2**, species **3** exhibits bond length distances and angles which are similar to those of corresponding octahedral complexes. Careful examination of Co(1)−O(x) (x = 1−6) distances and related angles tends to formulate a picture of a distorted octahedral geometry for **3**, with the O(1), O(3), O(4), and water anchor O(5) terminal atoms located in the equatorial plane, while the alcoholic oxygen O(2) and the water oxygen O(6) terminally occupy the axial positions of a compressed octahedron.

Given that there are two singly deprotonated quinate ligands bound to Co(II), the overall charge of the molecule is zero. The two water molecules bound to Co(II) along with the three water molecules of crystallization participate in hydrogen-bond formation, thus contributing to the formation of an extended and stable lattice in **3**.

Electronic Spectroscopy. The UV/visible spectrum of **1** was taken in water (Figure 4). The spectrum in the 200−800 nm range shows a well-formed major peak at

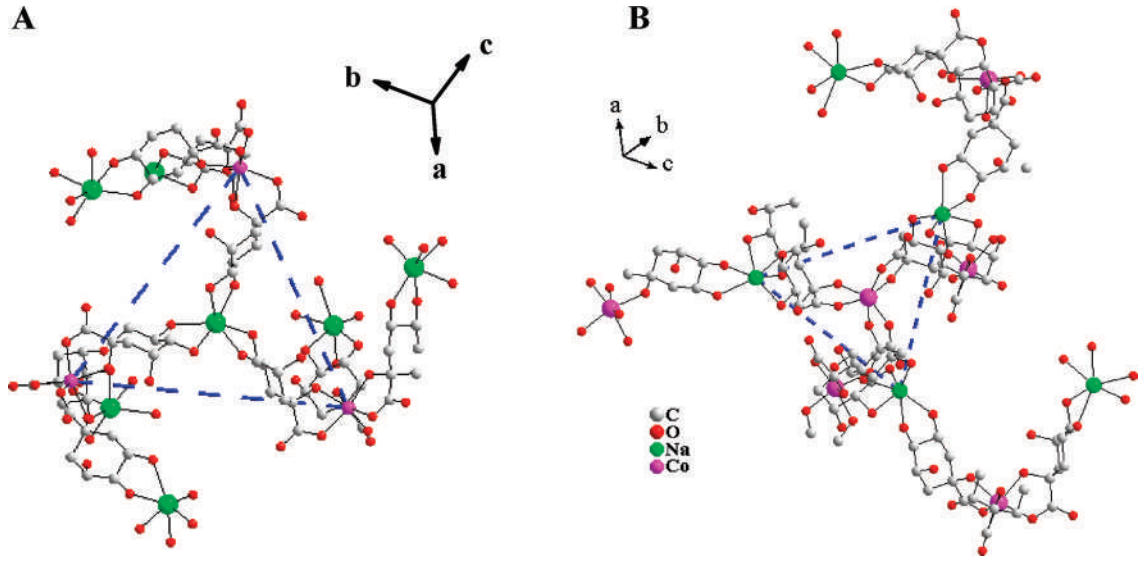

Figure 2. 3D infinite network crystal construction of **2** originating in Na^+-centered blade propellers. The position of the peripheral blades is perpendicular to the middle one. (2A) Na^+-centered Co(II) connectivity, (2B) Co(II)-centered Na^+ connectivity.

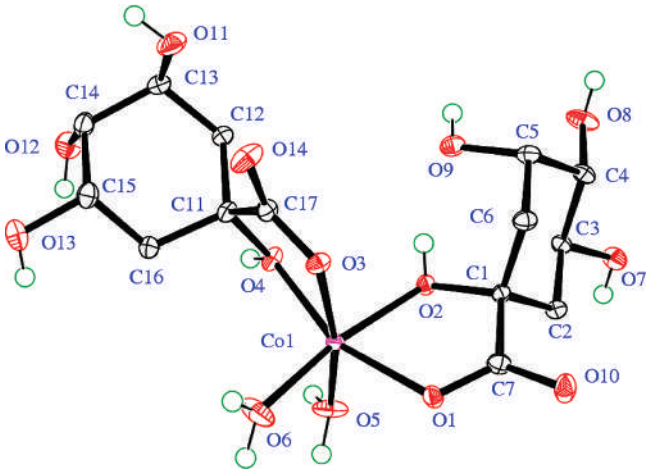

Figure 3. ORTEP diagram of the $[Co(C_7H_{11}O_6)_2(H_2O)_2]$ (**3**) molecule with the atom-labeling scheme (30% thermal probability ellipsoids).

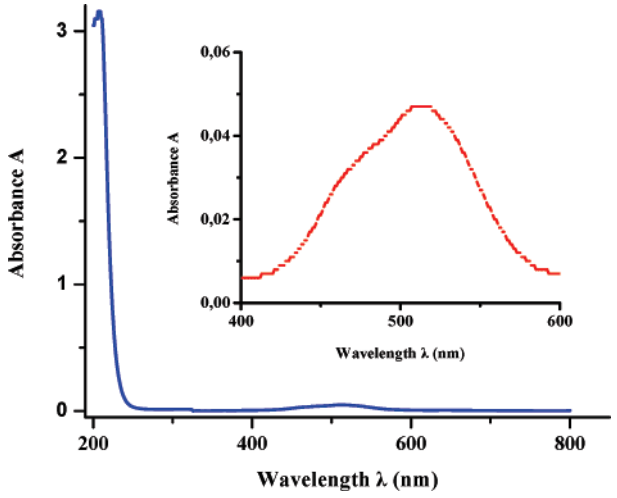

Figure 4. UV−visible spectrum of **1** in water.

λ_{max} = 514 nm (ε 12 M^{-1} cm^{-1}), with a shoulderlike band around λ = 460 nm ($\varepsilon \sim 7$ M^{-1} cm^{-1}). A distant band rising into the UV region appears at 206 nm (ε 770 M^{-1} cm^{-1}). The spectrum of **3** recorded in the 200−700 nm region exhibits almost identical features to those of **1**. The absorption features in the low-energy region are likely due to d−d transitions, which are typical for a Co(II) d^7 octahedral species.[45] The multiply structured band around 514 nm could be tentatively attributed to the $^4T_{1g} \rightarrow {}^4T_{1g}(P)$ transition. The observed multiple structure is in line with literature reports invoking (a) admixture of spin-forbidden transitions to doublet states derived from ^2G and ^2H, (b) spin−orbit coupling, and (c) vibrational or low-symmetry components, to account for the complexity of the spectrum.[46] No further assignments could be made in the absence of detailed specific work. The spectra of **1** and **3** in water are different from that of $Co(II)_{aq}$,[47] indicating the specific O-coordination sphere of Co(II) in solution.

FT-IR Spectroscopy. The FT-IR spectra of **1**−**3** in KBr exhibit strong absorptions for the carbonyls of the carboxylate groups in both the antisymmetric and symmetric vibration regions. The antisymmetric stretching vibrations $\nu_{as}(COO^-)$ appear around 1620 cm^{-1} (**1**), 1614 cm^{-1} (**2**), and 1596 cm^{-1} (**3**), whereas the symmetric stretches $\nu_s(COO^-)$ appear in the ranges 1452−1306 cm^{-1} (**1**), 1449−1274 cm^{-1} (**2**), and 1482−1303 cm^{-1} (**3**). The frequencies for all bands are shifted to lower values in comparison to those of free quinic acid. From that point of view, they indicate a change in the vibrational status of the quinate anion upon coordination to the metal ion. The difference, $\Delta(\nu_{as}(COO^-) - \nu_s(COO^-))$, is greater than 200 cm^{-1}, indicating the presence of deprotonated carboxylate groups free or coordinated to the metal ion in a monodentate fashion. The latter contention was further confirmed by the X-ray crystal structures of **1**−**3**. Similar trends in the frequencies for the carboxylate carbonyls have also been observed in the FT-IR spectra of other metal−quinate complexes as well as α-hydroxycarboxylate complexes with metal ions.[48]

Magnetic Susceptibility. $K[Co(C_7H_{11}O_6)_3]\cdot 3CH_3CH_2OH$ (1). Magnetic susceptibility measurements were carried out on compound **1** at different magnetic fields and in the temperature range 2.0−300 K. Figure 5A shows the $\chi_M T$ versus T susceptibility data at 0.5 T. The solid line represents the fit according to the following general Hamiltonian:

$$H = D\left[S_z^2 - \frac{1}{3}S(S+1)\right] + E(S_x^2 - S_y^2) + \mathbf{g}\mu_B H \cdot S \qquad (1)$$

where all of the parameters have their usual definitions and S = 3/2.

The $\chi_M T$ values decrease smoothly from 3.04 emu mol^{-1} K at 300 K to a value of 1.86 emu mol^{-1} K at 2.0 K. The high-temperature value of $\chi_M T$ is higher than 1.875 emu mol^{-1} K, the value that would be expected for a Co(II) system with an S = 3/2.[32,49] This behavior is consistent with the presence of a significant orbital contribution to the anisotropic nature of the investigated Co(II) system. The employed fitting model for the susceptibility data is shown in eq 1. The model takes into consideration (a) both the axial and rhombic parts of distortion of the crystal field (D, E) and (b) an isotropic g value, with the fitting results yielding the following parameters: D = 80(1) cm^{-1} and g = 2.56(1). The theoretical curve is shown as a solid line in the same figure. In that figure, different simulations with different values of the D parameter (and the same g value) are also shown. It must be pointed out that the sign of the D parameter along with the E parameter are not resolved from the magnetic measurements, while introduction of an

(45) Drago, R. S. In *Physical Methods in Chemistry*; W. B. Saunders Company: Philadelphia, PA, 1977; pp 359−410.
(46) Lever, A. B. P. In *Inorganic Electronic Spectroscopy*, 2nd ed.; Elsevier: Amsterdam, 1984; pp 480−490.
(47) (a) Figgis, B. N. In *Introduction to Ligand Fields*; Interscience Publishers: New York, 1966. (b) Jorgensen, C. K. *Adv. Chem. Phys.* **1963**, *5*, 33–146. (c) Ballhausen, C. J. In *Introduction to Ligand Field Theory*; McGraw-Hill Book Co.: New York, 1962.
(48) (a) Matzapetakis, M.; Raptopoulou, C. P.; Tsohos, A.; Papaefthymiou, B.; Moon, N.; Salifoglou, A. *J. Am. Chem. Soc.* **1998**, *120*, 13266–13267. (b) Matzapetakis, M.; Raptopoulou, C. P.; Terzis, A.; Lakatos, A.; Kiss, T.; Salifoglou, A. *Inorg. Chem.* **1999**, *38*, 618–619.
(49) Jankovics, H.; Daskalakis, M.; Raptopoulou, C. P.; Terzis, A.; Tangoulis, V.; Giapintzakis, J.; Kiss, T.; Salifoglou, A. *Inorg. Chem.* **2002**, *41*, 3366–3374.

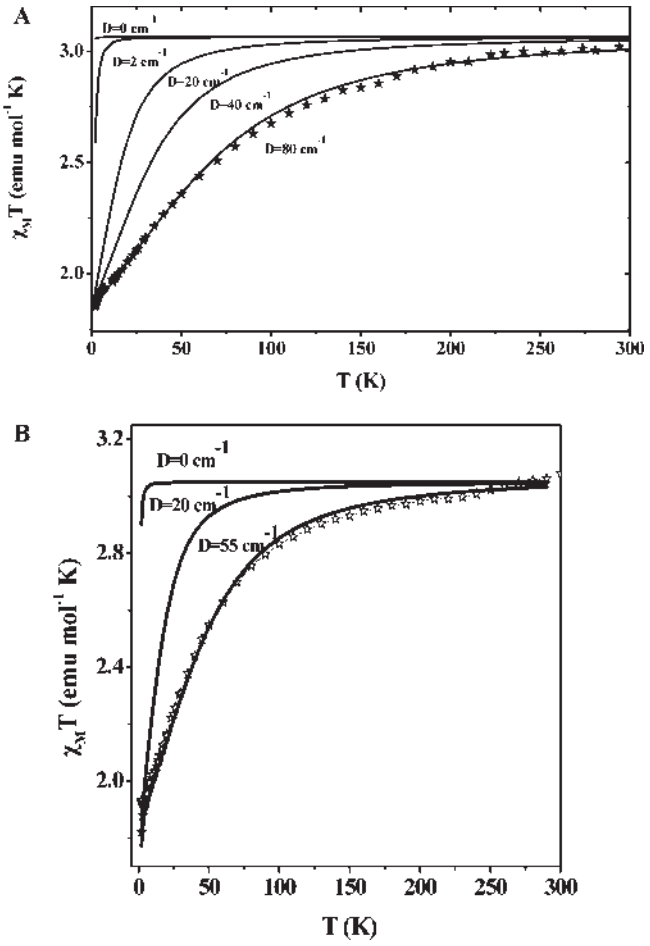

Figure 5. Temperature dependence of the magnetic susceptibility of **1** (A) and **3** (B), in the form of $\chi_M T$ versus T, in the temperature ranges 2.0−300 K (**1**) and 1.7−300 K (**3**) using an external magnetic field of 0.5 T and 0.7 T, respectively. The solid line represents the fitting results. (A) Different simulations of the susceptibility equation for different values of the D parameter ($D = 0, 2, 20, 40\ \text{cm}^{-1}$) are also shown as solid lines (see text). (B) Different simulations of the susceptibility equation for different values of the D parameter ($D = 0, 20\ \text{cm}^{-1}$) are also shown as solid lines (see text).

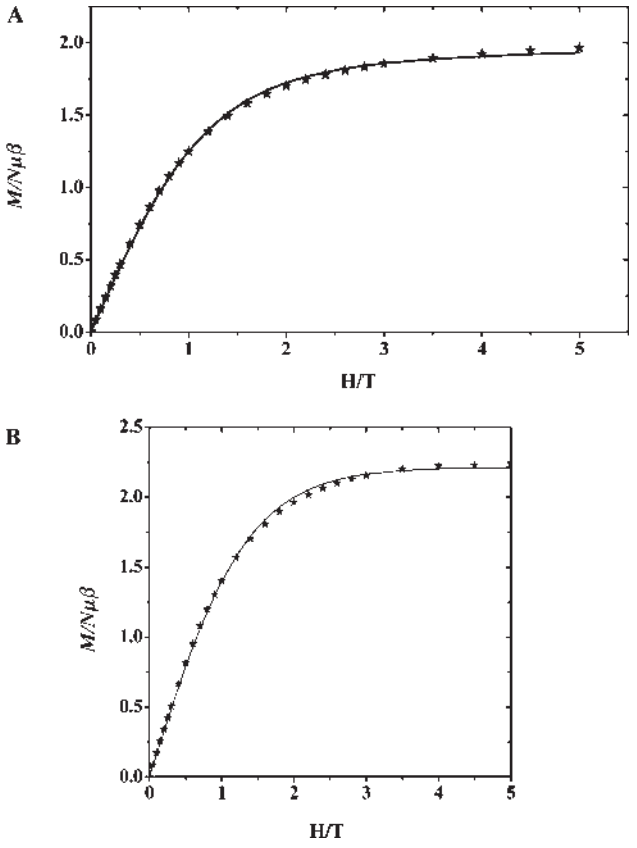

Figure 6. Magnetization of **1** (A) and **3** (B), in the form of $M/N\mu\beta$ versus H/T, at 2 K and in the field range 0−5 T. The solid line represents the theoretical Brillouin functions for an isolated $S = 1/2$ system with $g_{\text{eff}} = 4.0$ (**1**) and $g_{\text{eff}} = 4.33$ (**3**).

axial symmetry to the g parameter ($g_\perp$, $g_\parallel$) leads to no improvement of the fit. The large value of the D parameter is in accordance with the presence of octahedral Co(II), where the ground state doublet is well-isolated from the excited ones.[50a]

$[Co(C_7H_{11}O_6)_2(H_2O)_2]\cdot 3H_2O$ (3). Magnetic susceptibility measurements on compound **3** were carried out at different magnetic fields and in the temperature range 1.7−300 K. Figure 5B shows the $\chi_M T$ versus T susceptibility data at 0.7 T, while the solid line represents the fit according to the general Hamiltonian (eq 1) for $S = 3/2$.

The $\chi_M T$ values decrease smoothly from 2.98 emu mol^{-1} K at 300 K to 2.85 emu mol^{-1} K at 98 K and then more steeply to the value of 1.6 emu mol^{-1} K at 2.0 K. The high-temperature value of $\chi_M T$ is higher than 1.875 emu mol^{-1} K, the value that would be expected for a Co(II) system with an $S = 3/2$. The fitting results with the previously described magnetic model yield the following parameters: $D = 55(1)\ \text{cm}^{-1}$ and $g = 2.55(1)$. The theoretical curve is shown as a solid line in the same figure. Also shown in the same figure are different simulations with varying values of the D parameter (and the same g value). Here, too, the sign of the D parameter along with the E parameter are not resolved from the magnetic measurements, while the introduction of an axial symmetry to the g parameter ($g_\perp$, $g_\parallel$) leads to no improvement of the fit. The large value of the D parameter is in accordance with the presence of an octahedral Co(II) ion, where the ground state doublet is well-isolated from the excited ones.[50a]

Magnetization Studies. $K[Co(C_7H_{11}O_6)_3]\cdot 3CH_3CH_2OH$ (1). The magnetization data for **1**, in the form of $M/N\mu_B$ versus H/T, are shown in Figure 6A, for 2 K and in the field range 0−5 T. The solid line represents the theoretical magnetization curve for a system having a ground state with an effective spin $S = 1/2$ and effective g value equal to 4.0(1). The ground state of the free high-spin Co(II) ion in an octahedral environment is ^4F, but the orbital degeneracy is removed in an octahedral crystal field yielding one ^4A and two ^4T levels, with the lowest-lying state being a $^4T_{1g}$. The degeneracy of the $^4T_{1g}$ level is removed through the action of axial and rhombic distortions of the crystal field as well as through spin−orbit coupling. The overall effect of low-symmetry crystal-field components and spin−orbit coupling produces six Kramers doublets and results in a doublet ground state. Since (a) the same doublet energy level remains lowest in energy for all values of the applied field strength and (b) the energy

(50) (a) Boca, R. *Coord. Chem. Rev.* **2004**, *248*, 757–815. (b) Mateescu, A.; Raptopoulou, C. P.; Terzis, A.; Tangoulis, V.; Salifoglou, A. *Eur. J. Inorg. Chem.* **2006**, 1945–1956.

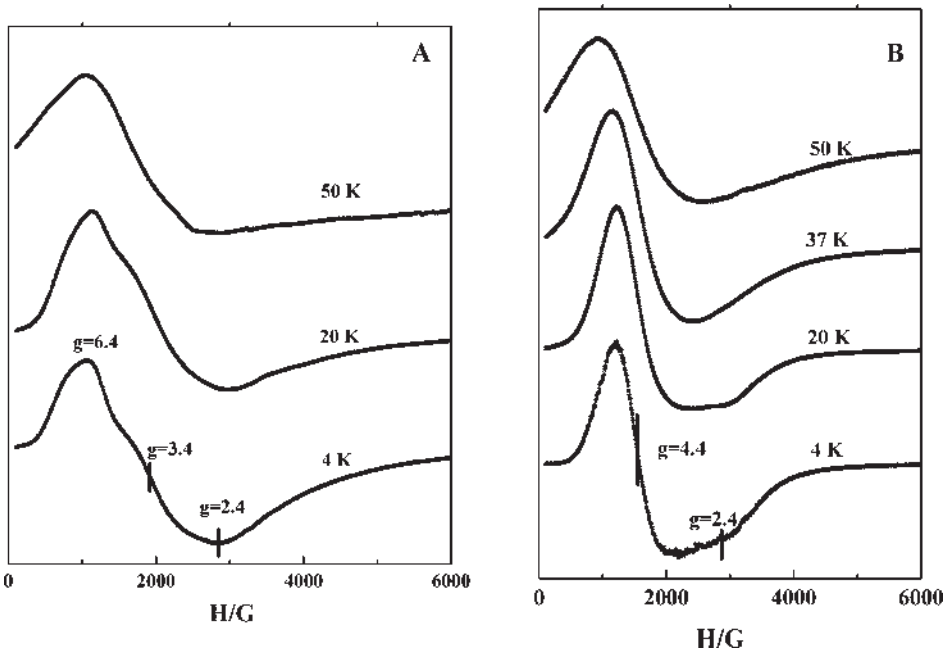

Figure 7. Temperature dependence of the powder (A) and water solution (B) X-band EPR spectrum of **1** in the field range 0−6000 G.

difference between the two lowest-lying doublets is relatively large with respect to the thermal energy present at low temperatures (< 30 K), the Co(II) system may be described as one having a ground state with an effective spin of $S = 1/2$. Since there is no discrepancy between the theoretical and the experimental curves, intermolecular interactions are of no importance in the low-temperature regime.

$[Co(C_7H_{11}O_6)_2(H_2O)_2]\cdot 3H_2O$ (3). The magnetization data for **3**, in the form of $M/N\mu_B$ versus H/T, are shown in Figure 6B, for 2 K and in the field range 0−5 T. The dotted lines represent the theoretical magnetization curves for a system having a ground state with an effective spin $S = 1/2$ and effective g value equal to 4.3(1). In this case as well, the Co(II) system may be described as one having a ground state with an effective spin of $S = 1/2$. Since there is no discrepancy between the theoretical and the experimental curves, intermolecular interactions are of no importance in the low-temperature regime.

EPR Spectroscopy. $K[Co(C_7H_{11}O_6)_3]\cdot 3CH_3CH_2OH$ (1). X-band EPR measurements were carried out in powder samples as well as in frozen solutions of **1** in water and are shown in Figure 7A and B, respectively. As a consequence of the fast spin−lattice relaxation time of high-spin Co(II), signals were observed only below 70 K. For the powder spectra, at temperatures $T < 20$ K, three resonances appear at ca. g_1, g_2, and $g_3 = 6.4$, 3.4, and 2.4, respectively, while for the solution spectra, the values are isotropic $g_{||}$ and $g_\perp = 4.4$ and 2.4, respectively. It is clear that the system does not retain its structure in solution since the two spectra (powder and solution) are different. A simulation[51] was carried out in order to derive the effective g values assuming a Hamiltonian formalism:

$$H = g_z\mu_B H_z S_z + g_x\mu_B H_x S_x + g_y\mu_B H_y S_y \qquad (2)$$

(51) Stoll, S. *Spectral Simulations in Solid-State EPR*, Ph.D. thesis, ETH Zurich, Zurich, **2003**.

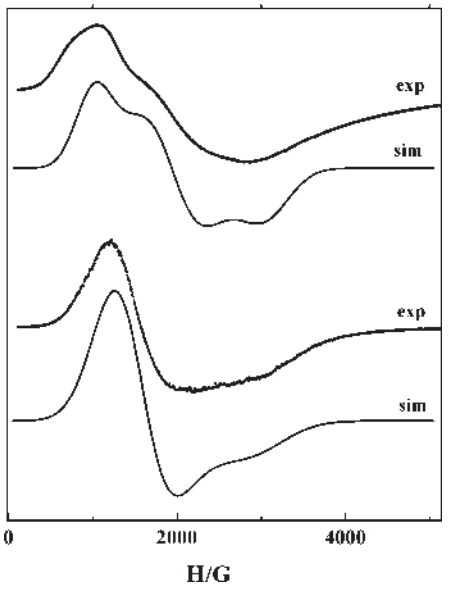

Figure 8. Powder (top) and solution (bottom) experimental and simulated spectra of **1** at 4 K. See text for details.

with an effective spin $S = 1/2$ and an anisotropic **g** tensor. The results are shown in Figure 8. An isotropic magnetic-field domain line width was used in both cases (lw = 35 G for the powder and lw = 75 G for the frozen solution), while the broadness of the spectra reveals the g strain effects. Gaussian distributions of the g-principal values were used, and the results are $\sigma g_x = \sigma g_z = 0.78$ and $\sigma g_y = 0.23$ for the powder and $\sigma g_x = \sigma g_y = \sigma g_z = 0.78$ for the frozen solution. The principal g values for the powder spectrum are $g_x = 3.4(1)$, $g_y = 2.2(1)$, and $g_z = 6.6(1)$ ($g_{eff} = 4.0(1)$) and for the frozen solution are $g_x = 4.6(1)$, $g_y = 4.6(1)$, and $g_z = 2.3(1)$ ($g_{eff} = 3.8(1)$). The dominant broadening effect emerges when the g strain is converted into B strain through the equation $\Delta B = -(h\nu/\mu\beta)(\Delta g/g^2)$, where the parameters have their usual meaning. Thus, the

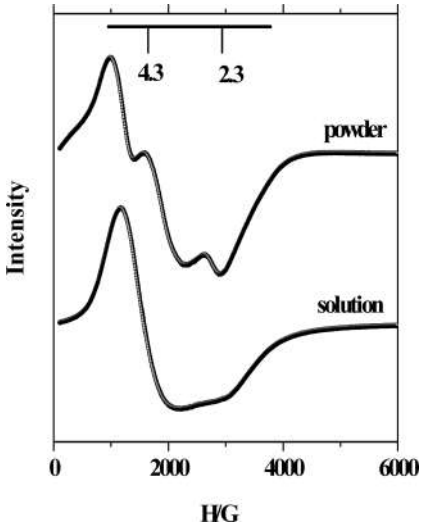

Figure 9. Powder (top) and water solution (bottom) X-band EPR spectrum of **3** at 4 K. See text for details.

largest and smallest g values of the powder and solution spectra have field widths that differ by an order of magnitude, thereby rationalizing the broad high-field features of the spectrum.

A very important feature of the Co(II) ion is the value of the effective g parameter, g_{eff}, extracted from the EPR measurements, as a result of which interesting comments can be made concerning the potential influence of intermolecular interactions. It has been shown[50b] that, for values of $g_{eff} > 4.33$ (in the EPR spectra of powder samples), the intermolecular interactions contribute significantly to the magnetic behavior of the system, while for all other cases ($g_{eff} < 4.33$), no significant intermolecular interactions are observed. According to our findings on the g_{eff} value of the powder EPR spectra, no significant intermolecular interaction appears; that is in accordance with the fitting results of the magnetization curve (a Brillouin function of an isolated $S = 1/2$ system could reproduce the magnetization using the same g_{eff} value obtained from the powder EPR spectra).

$[Co(C_7H_{11}O_6)_2(H_2O)_2]\cdot 3H_2O$ (3). X-band EPR measurements were carried out in powder samples as well as in frozen solutions of **3** in water and are shown in Figure 9. As a consequence of the fast spin−lattice relaxation time of high-spin Co(II), signals were observed only below 70 K. For the powder spectra, at temperatures $T < 25$ K, a rather complicated spectrum appears with many signals at low fields, making it quite difficult to follow the previously described simulation procedure, while it is clear that the system retains its structure in solution. In this case as well, the largest and smallest g values of the powder and solution spectra have field widths that differ by an order of magnitude, thereby rationalizing the broad high-field features of the spectrum.

Although it was not possible to derive a g_{eff} value from the powder EPR spectrum, the simulation of the magnetization curve gave a value of g_{eff} close to 4.33, indicating that the intermolecular interactions are not significant (a Brillouin function of an isolated $S = 1/2$ system could reproduce the magnetization).

Examination of the solution spectra of compounds **1** and **3** reveals that the spectra denote their correspondence

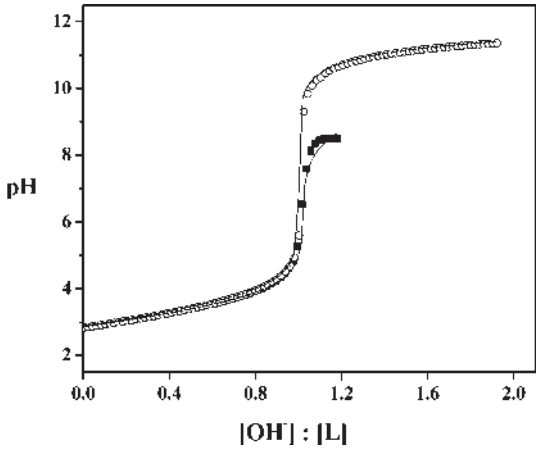

Figure 10. Potentiometric titration curves of free quinic acid (white circles; $c_{ligand} = 0.004976$ mol dm^{-3}) and Co(II)−quinic acid with molar ratios 1:3 (black squares); $c_{Co} = 0.001639$ mol dm^{-3}, $c_{ligand} = 0.004976$ mol dm^{-3}. Solid lines represent calculated curves.

to the same type of Co(II) ion configuration, namely that in species **3**. Further confirmation of the identity of **3** in solution comes from ESI-MS measurements on solutions arising upon dissolution of compound **3** in water ($m/z = 442$, $z = 1$, $[(M - 2H_2O) + H]^+$).

Speciation Studies. Potentiometric titrations of the ligand quinic acid alone, and Co(II) with D-(−)-quinic acid in various metal ion to ligand molar ratios were carried out. Some of the derived titration curves, both experimental and calculated, are shown in Figure 10. The titration curves were evaluated with different potential speciation models. In fact, three different potential models were considered and examined: (a) the first one includes the 1:2 species $[CoL_2]^0$, (b) the second one includes the 1:1 species $[CoL]^+$, and (c) the third included both species $[CoL]^+$ and $[CoL_2]^0$. The best fit between the experimental and calculated titration curves for the binary Co(II)−quinic acid system was obtained for the 1:1 and 1:2 cases (see Supporting Information). The third model encompassing both the 1:1 and 1:2 species was rejected by the computer program (PSEQUAD) during the computation process. In the 1:2 case, the adopted speciation model considered the species $[Co]^{2+}$, $[CoL_2]^0$ ($LH = C_7H_{12}O_6$; $L = C_7H_{11}O_6^-$), and $[CoL_2H_{-1}]^-$. The fit is reasonably good in the overall pH and concentration range used, demonstrating that the adopted speciation model is satisfactorily defined ($f = 0.027374$). Other complexes, like 2:1 Co(II)/quinate complexes or variably protonated and deprotonated species, were rejected by the computer program (PSEQUAD) during the computation process. The species emerging from the speciation distribution of the binary system are in line with the species synthesized and isolated in the solid state. The stability constants of the complexes formed are listed in Table 3. The uncertainties (3SD values) for the stability constants are given in parentheses. The pH range of the optimal formation of complexes is also reported. For the titratable quinate carboxylate group, the pK_a value of 3.34 was obtained and was found to be very close to the values reported by Clifford (3.40)[52] and Luethy-Krause et al.

(52) Clifford, M. *Tea Coffee Trade J.* **1987**, *159*, 35–39.

Table 3. Proton (log *K*) and Co(II) Complex Formation Constants (log β) of Quinic Acid (QA) at $I = 0.15$ (NaCl) and 25 °C[a]

	quinic acid	Co-QA	pH range for each species
log K(HL)	3.34(1)		
log β (CoL_2)		4.34(4)	entire domain
log β (CoL_2H_{-1})		−3.83(5)	>6.5
pK (CoL_2)		8.16	
fitting[b]		0.027374	
no. of pts.		300	

[a] Charges from the various species are omitted for clarity. [b] Goodness of fit between the experimental and the calculated titration curves expressed in milliliters of titrant.

(3.36).[53] For shikimic acid ((3R,4S,5R)-3,4,5-trihydroxy 1-cyclohexanecarboxylic acid), the pK_a value is 4.15. The presence of an alcoholic moiety in a position α to the carboxylate group of quinic acid increases its acid strength.

The titrimetric data were evaluated on the premise that complex formation between Co(II) and quinate proceeds through binding of the quinate carboxylate moiety and the alcoholic group. The titration curves in the absence and presence of Co(II) suggest formation of the complexes $[Co]^{2+}$ and $[CoL_2]^0$, in the acidic region up to pH 7, and of complex $[CoL_2H_{-1}]^-$ at pH values beyond 7 (Figure 11). Also, these studies suggest that this ligand reacts expediently with Co(II) ions, forming soluble metal chelate complexes.

The Co(II) ion is not sufficiently strong to deprotonate the alcoholic oxygens of the quinate ligand. Therefore, in congruence with the solid-state structure (Figure 3), which shows only the carboxylate group being deprotonated, the mononuclear complex $[CoL_2]^0$ contains the protonated ligand bound to the metal ion. This species forms in the entire pH investigated, with a maximum of 37% at pH 4.5−7, and it coexists with the hexa-aquo Co(II) species $[Co(H_2O)_6]^{2+}$ over the entire pH domain. The overall stability constant of the mononuclear complex $[CoL_2]^0$ (log β 4.35) is closer to that of similar complexes of Co(II) with some α-hydroxycarboxylic acids, such as 2-hydroxyacetic acid (glycolic acid; log β 3.01),[54] 2-hydroxypropanoic acid (lactic acid; log β 2.36),[55] 2-hydroxybutanoic acid (log β 2.38),[56] 2-hydroxy-2-methylpropanoic acid (2-hydroxyisobutyric acid; log β 2.43),[57] 2-hydroxy-2-phenylacetic acid (mandelic acid; log β 2.07),[58] and 2-amino-2-deoxy-D-glucopyranose (log β 4.09).[59]

At pH values beyond 7 in the binary Co(II)−quinic acid system, both (a) the mononuclear species $[CoL_2H_{-1}]^-$ and (b) the mononuclear species $[Co(OH)]^+$ are present. In the $[CoL_2H_{-1}]^-$ species, however, one of the two quinate ligands bound to the Co(II) is probably deprotonated at the alcoholic group adjacent to the carboxylate group, or one of the two coordinated water molecules

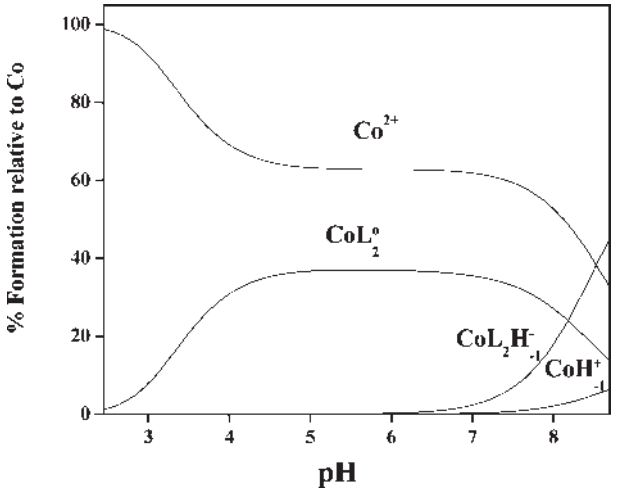

Figure 11. Speciation curves for complexes forming in the Co(II)−quinic acid system; $c_{Co} = 0.001667$ mol dm^{-3}, $c_{ligand} = 0.006635$ mol dm^{-3}. Charges are omitted for clarity.

(Figure 3) from $[CoL_2]^0$ is possibly deprotonated. The overall stability constant of the $[CoL_2H_{-1}]^-$ (log β −3.83) species is similar to the overall stability constant of the same species in the binary system Co(II)−2-amino-2-deoxy-D-glucopyranose (log β −3.89).[60] It could be noted that, in the system of Co(II) with 2-amino-2-deoxy-D-glucopyranose, the same species are present as in the Co(II)−quinic acid system. In the presence of 1-*O*-methyl-2-amino-2-deoxy-b-D-glucopyranoside, in addition to the CoL_2H_{-1} (log β −1.95) species, the CoL species (log β 2.93) forms as well.[57] Over the pH range 8.2−8.5, in the binary system of Co(II) with quinic acid, a precipitate appears and the pH rise ceases, most likely because OH^- ions are consumed toward formation of $Co(OH)_2$. The incipient precipitation at pH over 8.5 makes the observation of the next step doubtful, even in the presence of a higher ligand-to-metal molar ratio. Along the same lines, in the binary Co(II)−D-glucosamine system between pH 7 and 10, the CoL_2 (log β = 6.43) complex forms.[59] The presence of the hexa-aquo $[Co(H_2O)_6]^{2+}$ species, over the entire pH range investigated, is also noted. From the speciation curves of that system, it could be seen that the hexa-aquo $[Co(H_2O)_6]^{2+}$ species stays intact up to a pH around 11. In the presence of D-aldonic and D-alduronic acid, the free hexa-aquo $[Co(H_2O)_6]^{2+}$ species stays intact until pH 8.[61]

A similar speciation model arose for the 1:1 CoL case (see the Supporting Information). The adopted speciation model considered the species $[Co]^{2+}$, $[CoL]^+$ (LH = $C_7H_{12}O_6$; L = $C_7H_{11}O_6^-$), $[CoLH_{-1}]^0$, and $[CoH_{-1}]^+$. The fit is reasonably good in the overall pH and concentration range used, demonstrating that the adopted speciation model is satisfactorily defined ($f = 0.017991$). To this end, the two speciation models are reasonably good, and they suggest that additional information may be needed to select the one most representative of the solution speciation. ESI-MS spectroscopy was crucial in that respect, pointing out the species present in aqueous

(53) Luethy-Krause, B.; Pfenninger, I.; Landolt, W. *Trees−Struct. Funct.* **1990**, *4*, 198–204.
(54) Seys, R. G.; Monk, C. B. *J. Chem. Soc.* **1965**, 2452–2456.
(55) Larsson, R.; Nunziata, G. *Acta Chem. Scand.* **1972**, *26*, 1971–1980.
(56) Mayer, B.; Medancic, R.; Grabaric, B.; Filipovic, I. *Croat. Chem. Acta* **1978**, *51*, 151.
(57) Thun, G. H.; Guns, W.; Verbeek, F. *Anal. Chim. Acta* **1967**, *37*, 332–338.
(58) Matusinovic, T.; Filipovic, I. *Croat. Chem. Acta* **1985**, *58*, 227.
(59) Lerivrey, J.; Dubois, B.; Decock, P.; Micera, G.; Urbanska, J.; Kozlowski, H. *Inorg. Chim. Acta* **1986**, *125*, 187–190.
(60) Pusino, A.; Droma, D.; Decock, P.; Dubois, B.; Kozlowski, H. *Inorg. Chim. Acta* **1987**, *138*, 5–8.
(61) Escandar, G. M.; Sala, L. F.; Sierra, M. G. *Polyhedron* **1994**, *13*, 143–150.

solutions of Co(II) and quinic acid. Solution mixtures of Co(II) (solution A) and quinic acid (solution B) in molar stoichiometries of 1:1 and 1:2 showed that the species present is the 1:2 ($m/z = 442$, $z = 1$), very likely reflecting the CoL_2 species proposed by the aqueous speciation model discussed above (see the Discussion section).

Discussion

The Binary Co(II)−Quinate Synthetic Chemistry in Aqueous Media. The variable pH-dependent reactivity of $CoCl_2$ or $Co(NO_3)_2$ toward D-(−)-quinic acid exemplifies the chemical affinity of D-(−)-quinic acid for the divalent metal ion Co(II). Undoubtedly, the pH of the reaction solution assembled in each investigated case was crucial in promoting the requisite reactions to completion and affording crystalline products in a pure form, suitable for further characterization. The analytical, spectroscopic, and structural characterization of the derived materials reflected the physical and chemical properties of **1**−**3** and revealed a considerable number of structural details related to the aqueous reactivity of the examined binary system.

Specifically, the herein reported complexes **1**, **2**, and **3** provide the first examples of Co(II)−quinate families of species with the following arising properties: (a) Both classes of complexes are mononuclear, low molecular mass species synthesized and isolated through the reaction of Co(II) with an α-hydroxycarboxylate ligand. (b) In all cases, the quinate ligand binds Co(II) through the α-hydroxycarboxylate moiety, conferring stability to the arising species through chelation and formation of a five-membered cyclic ring. (c) In all three species, the quinate triol functionalities do not participate in metal ion binding. (d) In the course of the developing binary interactions, it appears that, in the presence of the metal ion Co(II), the alcoholic group adjacent to the carboxylic acid moiety retains its proton. Protonation of the alcoholic group in the α position to the carboxylate group has also been observed in the case of another α-hydroxycarboxylic acid, citric acid, upon binding to Co(II).[32]

The aforementioned structural features formulate the physical profile of complexes **1**, **2**, and **3** and reflect the respective chemical reactivity, because of which the title species emerged out of the reaction mixture in a pH-dependent fashion and crystallized out of solution in the presence of different bases (KOH, NaOH, and ammonia). This chemical specificity in corroboration with the presence of ethanol (precipitating solvent), expediting the crystallization and isolation of $[Co(C_7H_{11}O_6)_3]^-$, signifies the importance of lattice dynamics in achieving a stable lattice in **1** and **2** upon addition of the appropriate base (providing the necessary counterion). Enhancement of that solid state effect was achieved through the extended network of hydrogen bonds formed through interactions of the alcohol, water, and quinate ligand terminals in the absence or presence of K^+ and Na^+ counterions. In contrast to that, the mere presence of water molecules of crystallization in **3** was sufficient to deliver a stable crystalline lattice (with no ostensible participation of ammonium).

The physicochemical characterization of all three compounds emphasizes their distinct physicochemical properties in the solid state and in solution. Apart from the analytical and spectroscopic results corroborating the crystal structures of **1**−**3**, (a) the magnetic susceptibility studies reveal the presence of distinct high-spin Co(II) ionic forms in an octahedral crystal field, having a ground state with an effective spin $S = 1/2$ and effective $g = 4.0(1)$ (**1**) and 4.3(1) (**3**), and (b) the EPR signatures of the two classes of species are strongly indicative of their structural properties in the solid state. Essential to that effect is the contribution of EPR spectroscopy in deciphering the fate of **1** in solution. The data point to changes occurring in the structure of the complex in solution, an observation suggestive of dissociation of the complex in an aqueous medium at the autogenous pH and concurrent release of quinate. In this respect, **1** does not retain its structure in solution, thus emphasizing the importance of solid-state−solution structure correlation in studies targeting Co(II) binary interactions with physiological substrates (vide infra). The fact that the solution EPR spectrum of compound **1** dissolved in water is identical to that of compound **3** in water testifies to the identity of the species in water as compound **3**. That, however, is the same as species $[CoL_2]$, bearing a zero charge and suggested as a participant in the aqueous speciation scheme of the binary Co(II)−quinate system. Confirmation of the identity of compound **3** in solution comes from ESI-MS spectroscopy ($m/z = 442$, $z = 1$, $[(M - 2H_2O) + H]^+$), further supporting the EPR spectroscopic solution data.

The Chemical Link between Co(II)−Quinate Species. In a structurally diverse binary system, such as that of Co(II)−quinic acid, it is logical to look for structural connectivity between species of related structures. To this end, the two families of mononuclear species, i.e. (**1**,**2**) and **3**, reflect a pronounced difference between them that directly points to the additional quinate ligand in **1** and **2** that is absent in **3**. The absence of the quinate ligand in **3** is complemented by the presence of two coordinated water molecules. The presence of two singly deprotonated quinate ligands bound to Co(II), on the other hand, confers a zero charge on compound **3**. That, in conjunction with the presence of bound water molecules, reflects chemical characteristics that could promote further interactions (ternary) with third O-containing ligands−substrates of the same nature as quinic acid or different.

Led by the ostensible structural difference between the two classes of species, the synthetic transformation of **3** to **1** (and **2**) was pursued in a pH-specific fashion. The addition of one quinate ligand to **3** afforded **1**, the isolation of which was achieved under conditions employed in its original preparation. Positive identification of the product as compound **1** confirmed that (a) compound **3** is a precursor to compound **1** and (b) **1** and **3** are linked through a process reflecting the interactive chemistry of Co(II) with quinic acid in aqueous media under pH-specific conditions and leading to the isolation of distinct solid-state materials. The same behavior was confirmed in the case of **3** transforming to **2** by merely changing the base employed (from KOH to NaOH).

The Co(II)−Quinic Acid Binary System Speciation. A well-defined form of a metal−organic binary species such as **1**−**3** requires that an in-depth knowledge of its solution identity and properties be well established. To this end,

the aqueous solution study on the distribution of species arising in the binary system Co(II)−quinic acid (a) aids significantly in the understanding of the nature of various species forming as a function of pH and the stoichiometry of the partners involved and (b) provides a direct correlation of the physicochemical profile of the proposed species with the structure and properties of the species synthesized and characterized in this work (**1**−**3**). The potential speciation models, considered for evaluation, suggest the presence of either 1:1 CoL or 1:2 CoL_2 species in solution (among others). Combined solution speciation studies, EPR spectroscopy, and ESI-MS spectroscopy suggest that the likely speciation model is the one containing the 1:2 CoL_2 species. To this end, the likely species prevailing in the aqueous speciation of the investigated binary system bear a 1:2 Co/L stoichiometry. In line with this stoichiometry, mononuclear ($[CoL_2]^0$, $[CoL_2H_{-1}]^-$) species emerge as competent participants in the pH distribution. Of the two species, complex $[CoL_2]^0$ reflects the exact nature of the species synthesized and isolated in the solid state (**3**). Efforts are currently under way to synthesize and isolate species reflected in $[CoL_2H_{-1}]^-$. No $[CoL_3]^-$ species is suggested through the aqueous speciation, as that dissociates in solution to afford $[CoL_2]^0$.

Structural Diversity in the Aqueous Co(II)−Quinate Speciation. The presence of variable-nature species in the aqueous distribution of the binary Co(II)−quinate exemplifies the diversity of structures arising in solution as a result of the developing interactions between the two partners as a function of pH and molecular stoichiometry. Among the herein-described species, compound **3** represents an octahedral species (a) soluble in aqueous solutions, (b) with distinct geometrical characteristics, (c) bearing zero charge, and (d) essentially ternary in nature due to the presence of both quinate ligands and water molecules. These attributes, in connection with the structural differentiation of the component ligands of the complex, denote the chemical and structural factors that could influence the reactivity of Co(II) toward the aforementioned α-hydroxycarboxylate binder. To this end, the presence of a zero charge in compound **3** coupled with its structural attributes exemplifies the potential capabilities of Co(II) species to pursue ternary interaction chemistry with other low or high molecular mass congener ligands. Albeit speculative at this point, such chemistries could be envisaged as arising through substitution reactions involving the exchangeable water molecules bound to Co(II) in compound **3**. The nature of such complex ternary species arising in solutions is key to further understanding the reactivity of Co(II) toward hydroxycarboxylate-containing targets of variable preference for divalent metal ions.

Conclusions

The chemistry investigated in the binary Co(II)−quinic acid system (a) projects a clear view of the developing interactions, the complexity of the requisite speciation in aqueous media, and the diversity of species expected to arise as a function of pH and molecular stoichiometry; (b) defines the physicochemical attributes of two classes of Co(II)−quinate mononuclear species (**1**−**3**) isolated from aqueous solutions at specific pH values; (c) sheds light on specific structural features of the respective solid-state lattices of Co(II)−(O-containing) substrate materials **1**−**3**; and (d) relates to the transformation chemistry of binary and ternary metal−low molecular mass species that might be developing between Co(II), quinic acid, or other physiologically relevant hydroxycarboxylate binders and water. Efforts to unravel other novel elusive soluble forms of Co(II)-bearing quinate as well as other O-containing biologically relevant substrates of variable molecular mass are currently being pursued in our laboratories.

Acknowledgment. This research project was supported by a "Pythagoras" grant from the National Ministry of Education and Religious Affairs and a grant cofinanced by the E.U.-European Social Fund (75%) and the Greek Ministry of Development-GSRT (25%), Greece.

Supporting Information Available: X-ray crystallographic data in CIF format for $[K(Co(C_7H_{11}O_6)_3]\cdot 3CH_3CH_2OH$ (**1**), $Na[Co(C_7H_{11}O_6)_3]\cdot 3CH_3CH_2OH \cdot 2.25H_2O$ (**2**), and $[Co(C_7H_{11}O_6)_2(H_2O)_2]\cdot 3H_2O$ (**3**). The material is available free of charge via the Internet at http://pubs.acs.org.